

The high-light-induced protein SliP4 binds to NDH1 and photosystems facilitating cyclic electron transport and state transition in *Synechocystis* sp. PCC 6803

Luna Alvarenga-Lucius^{1*} , Markéta Linhartová^{2*} , Hendrik Schubert³ , Sandra Maaß⁴ , Dörte Becher⁴ , Wolfgang R. Hess⁵ , Roman Sobotka^{2,6}  and Martin Hagemann¹ 

¹Department of Plant Physiology, Institute of Biosciences, University of Rostock, D-18059 Rostock, Germany; ²Institute of Microbiology of the Czech Academy of Sciences, Opatovický mlýn, Třeboň 379 01, Czech Republic; ³Department of Aquatic Ecology, Institute of Biosciences, University of Rostock, D-18059 Rostock, Germany; ⁴Department of Microbial Proteomics, Institute of Microbiology, University of Greifswald, D-17489 Greifswald, Germany; ⁵Faculty of Biology, Genetics and Experimental Bioinformatics, University of Freiburg, Schänzlestr. 1, D-79104 Freiburg, Germany; ⁶Faculty of Science, University of South Bohemia, České Budějovice 370 05, Czech Republic

Summary

Authors for correspondence:

Luna Alvarenga-Lucius

Email: luna.alvarenga-lucius@uni-rostock.de

Martin Hagemann

Email: martin.hagemann@uni-rostock.de

Received: 2 December 2022

Accepted: 1 May 2023

New Phytologist (2023) **239**: 1083–1097

doi: 10.1111/nph.18987

Key words: acclimation, fluorescence, high light, NDH1, photosynthesis, superoxide dismutase, thylakoid.

- An increasing number of small proteins has been identified in the genomes of well-annotated organisms, including the model cyanobacterium *Synechocystis* sp. PCC 6803. We describe a newly assigned protein comprising 37 amino acids that is encoded upstream of the superoxide dismutase SodB encoding gene.
- To clarify the role of SliP4, we analyzed a *Synechocystis* *sliP4* mutant and a strain containing a fully active, Flag-tagged variant of SliP4 (SliP4.f).
- The initial hypothesis that this small protein might be functionally related to SodB could not be supported. Instead, we provide evidence that it fulfills important functions related to the organization of photosynthetic complexes. Therefore, we named it a small light-induced protein of 4 kDa, SliP4. This protein is strongly induced under high-light conditions. The lack of SliP4 causes a light-sensitive phenotype due to impaired cyclic electron flow and state transitions. Interestingly, SliP4.f was co-isolated with NDH1 complex and both photosystems. The interaction between SliP4.f and all three types of complexes was further confirmed by additional pulldowns and 2D-electrophoreses.
- We propose that the dimeric SliP4 serves as a molecular glue promoting the aggregation of thylakoid complexes, which contributes to different electron transfer modes and energy dissipation under stress conditions.

Introduction

The availability of an increasing number of complete genome sequences provided a blueprint for comprehensive analyses of biological functions. However, it has become clear that even among model organisms, many genes have remained without annotation or even entirely unidentified. Attempts to improve this situation led to the discovery of many small, nonprotein-coding RNAs in prokaryotic and eukaryotic genomes, which fulfill important regulatory functions (e.g. Hör *et al.*, 2020). In addition, many genes encoding for small proteins of < 100 amino acids have been overlooked because they were often below the cutoff of open-reading-frame (ORF)-predicting programs and/or more difficult to predict due to low conservation. However, there is an increasing body of evidence that small proteins fulfill diverse important functions in organisms, such as regulators of protein

functions, chaperons, and/or scaffolds for higher molecular complex formation (Hobbs *et al.*, 2011; Storz *et al.*, 2014).

Cyanobacteria are the only prokaryotes that perform oxygenic photosynthesis. They are often used as model organisms for basic photosynthesis research because eukaryotic algae and plants' evolution originate from an ancient cyanobacterium's endosymbiosis. Hence, many photosynthetic processes are well conserved between cyanobacteria and plants (Hohmann-Marriott & Blankenship, 2011; Ponce-Toledo *et al.*, 2017). One popular model strain for photosynthesis research is *Synechocystis* sp. PCC 6803 (hereafter *Synechocystis* 6803), because its genome became readily available in 1996 (Kaneko *et al.*, 1996). As for other model organisms, many small nonprotein-coding RNAs have been annotated in *Synechocystis* 6803 (e.g. Kopf *et al.*, 2014b). In addition, several small protein-encoding genes have been identified in its genome (Baumgartner *et al.*, 2016), but functional characterization has been done for only a few of these (Brandenburg & Klähn, 2020). For example, small proteins act as regulators of F₀F₁ ATP synthase (Song *et al.*, 2022), in salt acclimation (Klähn

*These authors contributed equally to this work.



et al., 2010) or primary carbon and nitrogen metabolism activities (Alvarenga *et al.*, 2020; Bolay *et al.*, 2021; Orthwein *et al.*, 2021) in *Synechocystis* 6803 and other cyanobacteria.

A particularly high number of small proteins are functionally related to photosynthesis, where they play important structural and functional roles as subunits of the Photosystem I (PSI), Photosystem II (PSII), and cytochrome *b₆f* complex in cyanobacteria as well as plants (reviewed in Baumgartner *et al.*, 2016). Moreover, cyanobacterial-specific subunits were assigned to NDH1-like complexes (Schwarz *et al.*, 2013; Wulffhorst *et al.*, 2014), which was recently named the photosynthetic complex I (Schuller *et al.*, 2019). Several distinct NDH1-like complexes differing in their composition and structure are involved in cyclic electron flow, dark respiration, and CO₂ conversion into bicarbonate as part of the cyanobacterial inorganic carbon-concentrating mechanism (reviewed in Hagemann *et al.*, 2021; Hualing, 2022; Laughlin *et al.*, 2020).

In the present study, we analyzed a small protein of 37 amino acids, initially identified as encoded on the high-light-induced RNA1 (Baumgartner *et al.*, 2016) in *Synechocystis* 6803. We provide evidence that this small protein fulfills important functions related to photosynthesis. Therefore, we named it a small light-induced protein of 4 kDa, SliP4. SliP4 is strongly induced under high-light conditions and associates with NDH1, PSII, and PSI complexes on thylakoid membranes. Mutation of the protein-coding part in the *sliP4* gene prevents state transitions and induction of cyclic electron flow, resulting in a mutant with high-light-sensitive phenotype. Collectively, our data indicate that SliP4 likely contributes to the association of NDH1 with PSI and/or PSII facilitating different electron transfer modes under stress conditions.

Materials and Methods

Construction of *Synechocystis* 6803 strains

The *Synechocystis* sp. PCC 6803 (Rippka *et al.*, 1979) substrain M (Trautmann *et al.*, 2012) was used as wild-type (WT; Supporting Information Table S1). To mutate genes, the kanamycin resistance gene *aphII* was inserted that was excised from pUC4K using *Bam*HI. The flanking sequences (500 bp in each direction) of the *sliP4* gene (nt positions 1606868–1606978) or of the intergenic region (nt positions 1607000–1607300) were obtained from total DNA of the *Synechocystis* 6803 WT via PCR using the primers 1849/1850 or 1958/1778 (Table S2). Overhanging *Bam*HI or *Bam*HI/*Nde*I sites were created in the respective 5' and 3' flanking regions. The resulting sticky ends were ligated with the *aphII* gene fragment in the backbone of plasmid pGEM-T (Promega). The plasmid pG_SliP4_5F/3F::Km was transformed into WT cells of *Synechocystis* 6803, and clones were selected on medium with kanamycin. Subsequent cultivation at 50 µg ml⁻¹ kanamycin resulted in complete segregation of the Δ *sliP4* and Δ *ig-sliP4-sodB* mutants. Genotyping was performed using primers listed in Table S2.

To generate the complementation strain Δ *sliP4*::*sliP4*-3xFlag (SliP4.f), the self-replicating plasmid pVZ322 expressing *sliP4*-3xFlag under control of its native promoter (Baumgartner

et al., 2016) was transferred into the Δ *sliP4* mutant via triparental mating with *E. coli* strain DH5 α /RP4. The selection of clones was done with 50 µg ml⁻¹ kanamycin/10 µg ml⁻¹ gentamycin. The same was done to obtain the mutants *Synechocystis* 6803 Δ PSII (Pakrasi *et al.*, 1988) and Δ PSI (Shen *et al.*, 1993). In these cases, the selection of clones was done with 50 µg ml⁻¹ kanamycin/20 µg ml⁻¹ chloramphenicol in BG-11 plates supplemented with 5 mM glucose.

Culture conditions, growth curves, and physiological analysis

All strains were precultivated in glass Erlenmeyer flasks (125 ml) filled with 40 ml of buffered BG11 medium (pH 8.0) without sodium bicarbonate (Rippka *et al.*, 1979) under the following conditions: 28 ± 2°C, continuous light of 50 µmol photons m⁻² s⁻¹. The growth experiments were conducted at 30°C in the Multi-Cultivator MC1000-OD (Photon Systems Instruments, Drásov, Czech Republic) with continuous illumination of 50 or 250 µmol photons m⁻² s⁻¹ and bubbling with 5% (v/v) CO₂-supplemented air. During 48 h preculture, cells were grown in BG11 aerated with 5% (v/v) CO₂-supplemented air in 350 ml column photobioreactors (580 × 30 mm) at 30°C under constant warm-white-light illumination of 100 µmol photons m⁻² s⁻¹. Mutant strains were grown in the presence of the respective antibiotics (50 µg ml⁻¹ kanamycin and/or 10 µg ml⁻¹ gentamycin) during the precultivation and without antibiotics during experiments. All experiments were performed with two biological replicates and repeated three times to confirm the results. The physiological analysis and photographs were done 48 h after inoculation under respective light treatments. Pigments were quantified by *in vivo* absorption measurements according to Sigalat & de Kouchkovsky (1975) as described in detail by Mantovani *et al.* (2022). Measurements of the oxygen-evolving activity were carried out in a Clark-type electrode connected to an oxygen monitor (Chlorolab 2 System; Hansatech, Norfolk, UK) using 2 ml of cyanobacterial culture (OD₇₅₀ c. 2) illuminated with saturating white light of 100 µmol photons m⁻² s⁻¹ at 30°C. The results were given as oxygen evolution per minute and per mg of chlorophyll *a* (nmol O₂ min⁻¹ mg⁻¹ Chl). The instrument was calibrated using a solution of sodium hydrosulfite and BG-11 medium to set 0% saturation.

Generation of recombinant SodB in *E. coli*

The WT *sodB* gene was obtained from *Synechocystis* 6803 DNA via PCR with the primer pair 2186/2187 (Table S2). The fragment was cut with *Nde*I/*Sa*I and ligated into plasmid pET28a(+) (Novagen, Darmstadt, Germany) cleaved with the same enzymes yielding plasmid pET28_SodB. The integrity of the vector was verified by plasmid DNA preparation, restriction, and sequence analyses. SodB protein was obtained in soluble form after expression in *E. coli* strain BL21 (DE3) harboring the vector pET28_SodB. The His-tagged recombinant SodB protein was purified from lysates using affinity chromatography on Ni-NTA columns (ProBond™ resin; Life Technologies) as described by Alvarenga *et al.* (2020). Bound



protein was then eluted three times with each 1 ml of 20 mM Tris buffer (pH 8) containing 300 mM imidazole. The elution fraction one was used for activity measurements and as a template for SodB antibody synthesis (Davids Biotechnologie GmbH, Regensburg, Germany). The SOD activity was estimated using Riboflavin/NitroBlue Tetrazolium (RF/NBT) assays according to Janknecht *et al.* (2007).

Sucrose gradient ultracentrifugation

SliP4.f cells and the knockout mutant $\Delta sliP4$ were cultivated at 350 $\mu\text{mol photons m}^{-2} \text{s}^{-1}$ in 200 ml BG11 until reaching OD₇₅₀ 1. The sample was immediately prepared without freezing or storage steps. Harvested cells were resuspended in 2 ml buffer (25 mM MES/NaOH pH 6.5; 10 mM MgCl₂; 10 mM CaCl₂) and mixed with glass beads in a 1 : 1 ratio. Cells were broken by six 20-s cycles using Mini-Bead Beater (BioSpec, Bartlesville, OK, USA) and cooled for 5 min after each cycle on ice. Broken cells were centrifuged for 30 min at 4°C and 25 000 g to pellet the membranes and to remove the soluble fraction. The pellet was resuspended in 250 μl of the buffer yielding a chlorophyll concentration of 600–700 $\mu\text{g ml}^{-1}$. Then, 150 μl of these samples was solubilized with 1% β -dodecyl-n-maltoside and 1% glyco-diosgenin for 30 min and centrifuged for 30 min at 4°C and 20 000 g to pellet nonsolubilized remnants. The supernatant was loaded on the top of a sucrose gradient prepared with a freeze-thawing method as follows. 12 ml of 20% sucrose solution in 25 mM MES/NaOH pH 6.5; 10 mM MgCl₂; 10 mM CaCl₂ buffer was frozen at –80°C and allowed to thaw in a cold room (8°C) for 2 h. The samples were loaded on the gradients and centrifuged for 18 h using an ultracentrifuge (SW 40 Ti rotor, 285 000 g, 4°C, Optima XPN-90; Beckman Coulter, Indianapolis, IN, USA).

Protein analysis by polyacrylamide gel electrophoresis and immunodetection

Proteins were separated by standard sodium dodecyl sulfate polyacrylamide gel electrophoresis (SDS-PAGE) (12% acrylamide) using the minigel system (Bio-Rad). The separated proteins were either stained with Coomassie brilliant blue or transferred onto polyvinylidene difluoride (PVDF) membranes (Hybond P, Amersham, Chalfont, UK) using electro-blotting. Total protein extracts (10 μg) from cells of WT, $\Delta sliP4$, or $\Delta sliP4::sliP4$ -3xFlag (SliP4.f), which were cultivated at 250 $\mu\text{mol photons m}^{-2} \text{s}^{-1}$ of continuous light, were used for western blotting. SodB was detected with a specific antibody against recombinant SySodB generated in our laboratory and synthesized by Davids Biotechnologie GmbH. The Flag-tagged SliP4 protein SliP4.f was detected with a commercial anti-Flag-tag antibody (Monoclonal ANTI-Flag M2-Peroxidase (HRP); Sigma-Aldrich).

Isolation of SliP4-Flag complexes

SliP4.f cells were cultivated photoautotrophically in cuvette bioreactors with 2.4 l BG11 medium at 28°C and 350 $\mu\text{mol photons m}^{-2} \text{s}^{-1}$ until reaching OD₇₅₀ c. 1. To cultivate

cells producing SliP4.f but lacking PSI or PSII, strains were grown in BG11 medium supplemented with 5 mM glucose in 10 l flasks at 28°C and 5 $\mu\text{mol photons m}^{-2} \text{s}^{-1}$. To induce expression of SliP4.f, the irradiance was increased to 150 $\mu\text{mol photons m}^{-2} \text{s}^{-1}$ during the last hour of cultivation. Cells were harvested by centrifugation, washed with, and resuspended in a thylakoid buffer containing 25 mM MES/NaOH, pH 6.5, 10 mM MgCl₂, and 25% glycerol. The isolation of membranes and Flag pull-down assays was performed according to Koskela *et al.* (2020). Briefly, the isolated membranes were solubilized with 1% β -dodecyl-n-maltoside and the amount corresponding to 7 mg of chlorophyll was loaded onto a column containing 150 μl of the anti-Flag-M2 agarose resin (Sigma-Aldrich). The resin was then washed with 20 ml of the thylakoid buffer containing a mixture of 0.02% β -dodecyl-n-maltoside and 0.02% glyco-diosgenin to remove nonspecific protein interactions. SliP4.f and associated proteins were finally eluted with 300 $\mu\text{g ml}^{-1}$ of 3xFlag peptide (Sigma-Aldrich) in 300 μl of the thylakoid buffer containing 0.02% β -dodecyl-n-maltoside and 0.02% glyco-diosgenin. The elution step was repeated once, and the eluted proteins were concentrated using Amicon Ultra 50 K (Merck KGAA, Darmstadt, Germany) to a final volume of 100 μl .

2D blue native and clear native/SDS-PAGE and immunoblotting

To analyze solubilized protein complexes with blue native (BN)/SDS-PAGE, samples containing 6 μg of chlorophyll were solubilized with 1% β -dodecyl-n-maltoside for 5 min and then centrifuged at 20 000 g, 4°C for 5 min. The supernatant was gently mixed with 1/10 of the sample volume of Coomassie loading dye solution and separated at 4°C using a one-dimensional BN 4–14% gradient acrylamide gel (Komenda *et al.*, 2012). After the run, single lanes were cut into stripes and each denatured with 3 ml of 25 mM Tris/HCl buffer, pH 7.5 containing 2% SDS and 1% dithiothreitol for 20 min at room temperature. In the second dimension, the stripes were then placed on the top of the 16–20% denaturing SDS gel containing 7 M urea (Dobáková *et al.*, 2009). Proteins separated in the 2D gel were stained with Coomassie brilliant blue or SYPRO Orange (Sigma). For the immunodetection, proteins were transferred from the SDS gel onto a PVDF membrane (Immobilon-P; Merck Millipore), which was incubated with primary antibodies and then with a secondary antibody conjugated with horseradish peroxidase (Sigma-Aldrich). The antibody against IsiA has been described in Wilson *et al.* (2007). NdhH was detected with an anti-NdhH antibody from Agrisera (AS164065; Agrisera, Vännäs, Sweden). For clear native (CN)/SDS-PAGE, samples (50 μl) were mixed with 1% amphipol A8-35 (Anatrace, Maumee, OH, USA), incubated for 10 min on ice, and separated in 4–14% or 4–8% CN-PAGE according to Kameo *et al.* (2021). For the second dimension, the cut CN gel stripes were processed as described for the BN stripes.

Mass spectrometry for protein identification

For the identification of Coomassie-stained protein bands/spots by mass spectrometry, excised gel pieces were treated as described by Bonn *et al.* (2014). Briefly, gel pieces were de-stained and



dried in a vacuum centrifuge before proteins were in-gel digested with trypsin. The resulting peptides were eluted and subjected to mass spectrometry. LC–MS/MS analyses were performed with an EASY-nLC 1000 liquid chromatography system coupled to an LTQ Orbitrap Velos (Thermo Fisher Scientific, Waltham, MA, USA). Tryptic peptides were loaded on a self-packed analytical column (OD 360 μm , length 20 cm) filled with 3 μm diameter C18 particles (Dr Maisch HPLC GmbH, Ammerbuch, Germany). Peptides were then eluted using a binary nonlinear gradient of 5–99% acetonitrile in 0.1% acetic acid over 157 min at a flow rate of 300 nl min^{-1} and subjected to electrospray ionization-based MS. A full scan in the Orbitrap with a resolution of 30 000 was followed by collision-induced dissociation (CID) of the 20 most abundant precursor ions. MS/MS experiments were acquired in the linear ion trap.

Resulting raw files were searched with MAXQUANT (v.2.0.3.0; Cox & Mann, 2008) against a database of *Synechocystis* 6803 downloaded from Uniprot on 18/12/2019 and supplemented with sequences of Flag-tagged, nonannotated small proteins (3510 entries). Common laboratory contaminants and reversed sequences were included by MAXQUANT. Search parameters were set as follows: Trypsin/P specific digestion with up to two missed cleavages, methionine oxidation, and N-terminal acetylation as variable modification. The FDRs (false discovery rates) of protein and PSM (peptide spectrum match) levels were set to 0.01. The MS data have been deposited to the ProteomeXchange Consortium via the PRIDE partner repository (Vizcaino *et al.*, 2016) with the dataset identifier PXD036788.

Fluorescence measurements

PSII fluorescence and PSI redox status were recorded simultaneously in a 1-cm cuvette with a DUAL-PAM 100, equipped with the optical unit ED-101US/MD and the measuring heads DUAL-E and DUAL-DR (Walz GmbH, Effeltrich, Germany). For recording slow kinetics of P700 absorbance changes and PSII fluorescence, the following settings were used: measuring light PSII 25 $\mu\text{mol photons m}^{-2} \text{s}^{-1}$, actinic light PSI (red LED) 805 $\mu\text{mol photons m}^{-2} \text{s}^{-1}$, actinic far-red light 255 $\mu\text{mol photons m}^{-2} \text{s}^{-1}$. PSII and PSI quantum yields were calculated by means of the in-built software (DUAL-PAM v.3.18) after irradiance titration (0, 6, 15, 50, 101, 140, 251, 406, 646, and 1011 $\mu\text{mol photons m}^{-2} \text{s}^{-1}$). Samples were preincubated for at least 30 min in darkness before the measurements.

Samples, kept in Pasteur capillaries, were first exposed to darkness for 30 min. Subsequently, dark-exposed samples were either exposed to far-red light (100 $\mu\text{mol photons m}^{-2} \text{s}^{-1}$ intensity, wavelength 730 nm) for 20 min or orange light (100 $\mu\text{mol photons m}^{-2} \text{s}^{-1}$ intensity, wavelength 600–630 nm) for 20 min. Afterward, cells incubated in darkness or to either far-red or orange light were frozen in liquid nitrogen. Low-temperature (77 K) fluorescence emission spectra were recorded with a Hitachi F4010 (Hitachi Inc., Tokyo, Japan) spectrofluorometer. Excitation wavelength was set at 600 nm with a bandpass of 10 nm, allowing direct measurement without the use of cutoff filters. Spectra shown were normalized to the long-wavelength emission peak at *c.* 722 nm.

Results

Sequence and expression characteristics of SliP4

In the present study, we aimed to analyze the 37 amino acid small protein SliP4 (small light-induced protein of 4 kDa), which is encoded on the high-light-inducible RNA1 localized upstream of the gene *sodB* (*slr1516*; Baumgartner *et al.*, 2016; Fig. 1). Only the respective gene in *Synechocystis* sp. PCC 6714 has previously been annotated in its genome sequence (gene D082_13860; Kopf *et al.*, 2014a), while the homolog in *Synechocystis* 6803 was recently predicted and validated experimentally (Baumgartner *et al.*, 2016). Although not annotated, further *sliP4* homologs can be identified by tBLASTn searches in the genomes of *Synechocystis* sp. CACIAM 05 (GenBank accession CP019225), IPPAS B-1465 (Genbank accession CP028094), PCC 7338, and PCC 7339 (Jeong *et al.*, 2021; and Genbank accessions CP054306 and CP063659). The corresponding SliP4 proteins are highly conserved in all *Synechocystis* spp. (Fig. 1a). They possess a putative transmembrane domain at the N terminus followed by a positively charged disordered C terminus. Outside *Synechocystis*, only a few similar proteins were detected, which share the presence of a transmembrane helix followed by a short tail of charged amino acid residues (see Fig. S1). In *Synechocystis* 6803, the *sliP4* gene is most highly expressed not only under high-light conditions but also under other stress regimes, such as low CO₂ conditions or cold stress (Fig. 1c). The downstream gene *sodB* that belongs to a separate transcriptional unit (TU; Fig. 1b) encodes the iron-containing superoxide dismutase SodB in *Synechocystis* 6803, which fulfills important functions to prevent oxidative stress damage in cyanobacteria as well as in plants (Fridovich, 1989). Accordingly, the *sodB* gene is also induced under many stress conditions, including high light, as found for *sliP4* (Fig. 1c).

Phenotyping of mutant strains

To study the function of SliP4, two knockout mutants were initially generated. First, only the protein-coding part of *sliP4* was inactivated by interposon mutagenesis giving rise to the strain Δ *sliP4*. Second, the protein-coding part of *sliP4* was left intact, while the intergenic, RNA-encoding region between the *sliP4* protein-coding sequence and *sodB* was deleted (Δ *ig_sliP4_sodB* strain). The two deletion mutants allowed us to distinguish whether the small protein SliP4 or the longer RNA transcribed from the TU1647 is functionally relevant, that is, to rule out that the TU1647 encodes a dual-function RNA. Genotyping validated that the WT *sliP4* gene in Δ *sliP4* or the intergenic region in Δ *ig_sliP4_sodB* was completely replaced by the mutated gene copies in both mutants (Fig. S2), indicating that the SliP4 protein and/or the RNA part are not essential under standard growth conditions. Finally, the protein-coding part of *sliP4* was fused with a segment encoding a C-terminal 3 \times Flag tag. This construct was expressed under the control of its native promoter on the self-replicating plasmid pVZ322 for ectopic expression of SliP4 in the mutant Δ *sliP4*. This generated the complementation strain Δ *sliP4*::SliP4 expressing Flag-tagged SliP4 (SliP4.f).



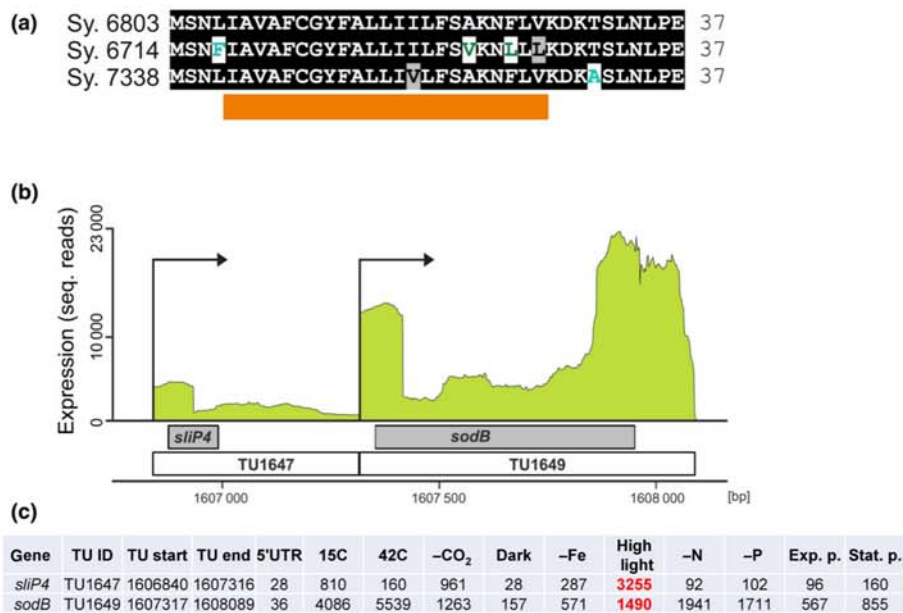


Fig. 1 Small protein Slp4 in *Synechocystis* sp. PCC 6803. (a) Slp4 in *Synechocystis* 6803 (identical proteins are encoded in *Synechocystis* sp. CACIAM 05 and IPPAS B-1465) and its homologs in *Synechocystis* sp. PCC 6714 and *Synechocystis* sp. PCC 7338 (identical Slp4 encoded in PCC 7339) are 37 amino acids long (black, identical amino acids; grey, similar amino acid exchange; white, non-conserved amino acids) and share the presence of a single predicted transmembrane helix (orange bar underneath). (b) Transcriptome coverage around the *slp4* and downstream located *sodB* genes. Mapped initiation sites of transcription are indicated by arrows; the lengths and numbers of the respective transcriptional units (TU1647 and TU1648) are indicated below. The positions within the chromosome are plotted on the x-axis, and the read counts are on the y-axis (data replotted from Kopf *et al.*, 2014b). (c) Expression of *slp4* and *sodB* under 10 different growth conditions based on previous dRNA-seq analysis (Kopf *et al.*, 2014b). These conditions were as follows: cold (15°C) and heat (42°C) for 30 min each; -CO₂, cells were washed three times with Ci-free BG11 and cultivated further for 20 h; dark incubation for 12 h; -Fe, iron was removed by adding the iron-specific chelator desferrioxamine B and continued cultivation for 24 h; high light, 470 μmol photons m⁻² s⁻¹ for 30 min (highlighted in red); -N, -P cells were washed three times with nitrogen-free or phosphate-free BG11 and cultivated further for 12 h; exponential phase (Exp. p.) and stationary phase (Stat. p.). Values indicate normalized sequencing read counts for the primary 5' end ×50. The lengths of the respective 5'UTRs and the TU start and end positions are given for the *Synechocystis* 6803 chromosome sequence available in Genbank under accession no. NC_000911.

These mutant strains were then compared with WT under different growth conditions. Under standard conditions, all strains showed similar growth as the WT (Fig. 2b). Because the *slp4* gene is induced under high light, we transferred the cultures from standard to high-light conditions. The mutant Δ *slp4* displayed slower growth and a bleaching phenotype when light exceeded 200 μmol photons m⁻² s⁻¹ (Fig. 2a,b). This phenotype was completely recovered in the complementation strain Δ *slp4*::Slp4.f, and it was not observed for the Δ *ig_slp4_sodB* mutant with the deleted intergenic region. These results indicate that the small protein Slp4, not the longer RNA transcribed from the TU1647, is essential for the high-light acclimation in *Synechocystis* 6803. Consistent with the slower growth and bleaching phenotype, the mutant Δ *slp4* showed decreased photosynthetic activities and less pigmentation than all other strains (Fig. 2c).

Effect of Slp4 on the expression of *sodB* and the SodB *in vitro* activity

Due to the proximity of the genes *slp4* and *sodB*, we initially hypothesized that these two proteins might be somehow functionally related. SodB has often been described as a universal stress protein responding to many growth-disturbing conditions that induce oxidative stress, such as high light, iron starvation, or salt stress (e.g. Hagemann, 2011). Hence, the high-light-induced

Slp4 could be involved in regulating *sodB* expression. Moreover, the predicted transmembrane helix in the Slp4 protein (Fig. 1a) led us to assume that it could also serve as a scaffold protein anchoring the soluble SodB protein or another oxidative stress protection protein at the membrane in the vicinity to reactive oxygen species-producing protein complexes, for example, PSI. First, we tried to verify a direct protein/protein interaction between recombinant SySodB and Slp4.f or synthetic Slp4 peptide. However, these attempts never showed any sign of a direct protein/protein interaction between these two partners (data not shown). Moreover, no significant changes in the activity of recombinant SySodB protein were found in the presence or absence of added synthetic Slp4 (Fig. S3A). Finally, the SodB abundance was unchanged in cells of the WT and the different mutants under high-light conditions (Fig. S3B). However, more experiments are necessary to ultimately rule out that Slp4 directly interacts with SodB or influences its activity or localization in *Synechocystis* 6803.

Slp4.f co-localizes with photosynthetic complexes in thylakoid membranes

To verify that Slp4 is membrane-associated, extracts from cells expressing Slp4.f were analyzed in sucrose gradients and blue-native-(BN)-gels. These experiments revealed that Slp4 is found



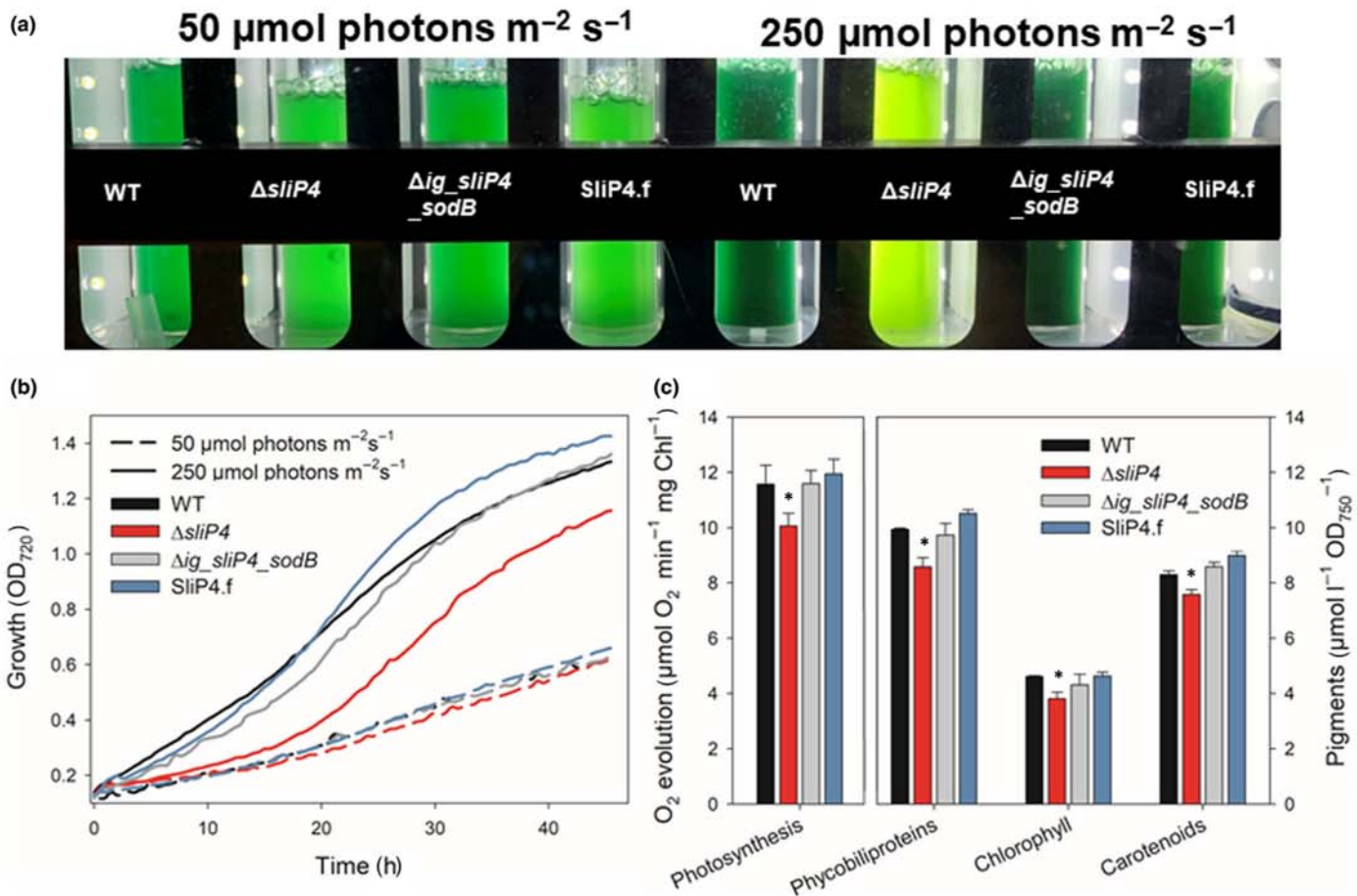


Fig. 2 High-light-sensitive phenotype of the *Synechocystis* sp. PCC 6803 mutant ΔsliP4 . (a) Appearance of the wild-type (WT) and the strains ΔsliP4 , $\Delta\text{ig_sliP4_sodB}$, and $\Delta\text{sliP4}::\text{sliP4-3}\times\text{Flag}$ (SliP4.f) after 48 h growth at 50 or 250 $\mu\text{mol photons m}^{-2} \text{s}^{-1}$. (b) Growth curves for the different strains as an increase in optical density of 720 nm (OD₇₂₀) under 50 or 250 $\mu\text{mol photons m}^{-2} \text{s}^{-1}$ in the multicultivator system with 5% CO₂ supplemented air (one representative growth curve is shown). (c) Oxygen-evolving activity and pigmentation of the different strains after 48 h growth at 250 $\mu\text{mol photons m}^{-2} \text{s}^{-1}$. Significant difference according to Student's *t*-test. Mean values \pm SE are shown *, $P < 0.01$.

in thylakoid membranes (data not shown). To identify putative protein partners of SliP4, we first separated solubilized membrane protein complexes from high-light-exposed SliP4.f cells by 2D BN/SDS-PAGE. The resulting gel was stained with SYPRO Orange, blotted, and the SliP4.f protein detected by anti-Flag antibody (Fig. 3). No Flag signal was detected in the control strain lacking SliP4 (Fig. S4). Interestingly, the SliP4.f protein (6.5 kDa) appeared on the denatured SDS gel as a double band, the upper band with a mass of *c.* 14 kDa. It is, therefore, very likely that SliP4.f forms a dimer of remarkable stability. In BN gels, SliP4.f migrated in at least four different bands of high molecular mass, which indicated that this small protein associates with some other membrane complexes (Fig. 3). The uppermost band (#1) was close to the top of the gel with an apparent mass > 1 MDa, while the band #2 migrated together with trimeric PSI (PSI(3)). The SliP4.f band #3 co-localized with monomeric PSI (PSI(1)) and/or monomeric PSII (PSII(1)), and the mass of band #4 we estimated *c.* 150 kDa. To further analyze the association of SliP4 with different photosynthetic complexes, particularly in the highest mass complex #1 (Fig. 3), sucrose gradient centrifugation was applied to separate the solubilized membranes from the

Synechocystis 6803 strain SliP4.f (Fig. 4) and the mutant strain ΔsliP4 (Fig. S5).

The total protein extract was separated into 15 fractions containing protein complexes of different masses. All fractions were subsequently loaded on the clear-native (CN)-PAGE (Fig. 4). The CN gel was scanned in true colors, blotted, and the SliP4.f detected by anti-Flag antiserum. Because we used a relatively low concentration of sucrose (see the Materials and Methods section), PSI(3) complexes (*c.* 1 MDa) occurred in the middle of the gradient (fraction 7; Fig. 4). Interestingly, SliP4.f was present also in fractions containing larger complex(es) than PSI(3), which was consistent with BN-PAGE of the solubilized membranes (band #1, Fig. 3). By contrast, especially the uppermost complexes above PSI(3) were missing when analyzing protein extracts from the mutant ΔsliP4 (Fig. S5). The second major accumulation of SliP4.f in the sucrose gradient was present in fractions 9 and 10. On the CN gel, SliP4.f in these fractions migrated mostly above the PSI(1) (Fig. 4). No Flag-specific signal was detected in a control blot from the ΔsliP4 strain (Fig. S5).

Fractions 7 and 9 were separated again by CN-PAGE followed by SDS-PAGE in the second dimension, stained with SYPRO

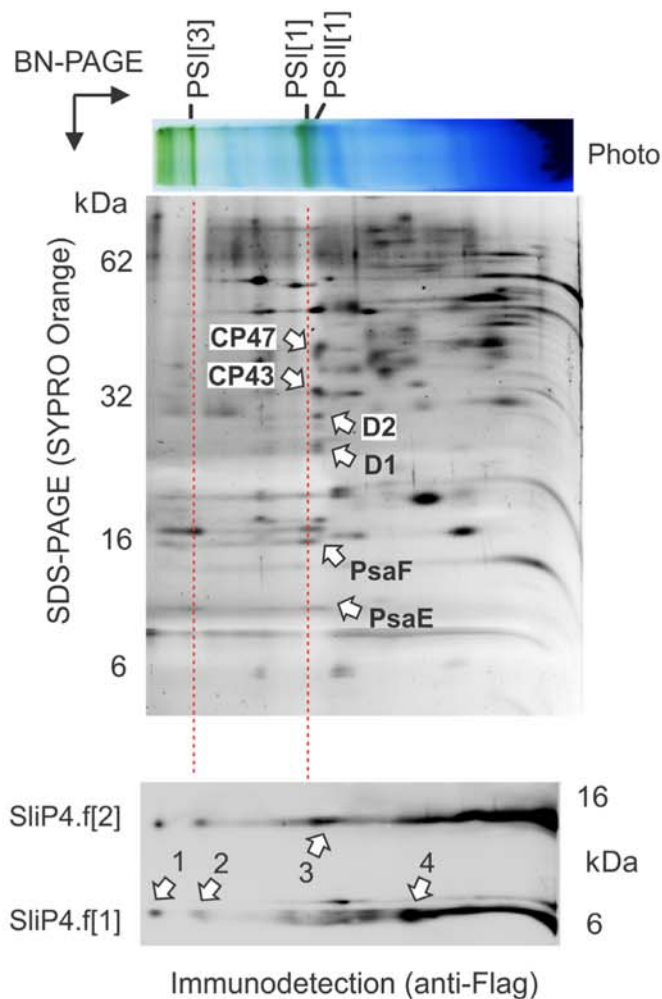


Fig. 3 2D-analysis of membrane proteins of the *Synechocystis* sp. PCC 6803 SliP4.f strain. SliP4.f-expressing cells were grown for 48 h at $350 \mu\text{mol photons m}^{-2} \text{s}^{-1}$ and harvested at $\text{OD}_{750\text{nm}} \approx 0.5$. The isolated membranes ($6 \mu\text{g}$ of chlorophyll) were analyzed by Two-dimensional-blue-native/sodiumdodecylsulfate polyacrylamide gel electrophoresis (2D-BN/SDS-PAGE). After the first dimension, the gel was photographed (Photo) and separated in the second dimension. The 2D gel was stained using SYPRO Orange and blotted to a polyvinylidene difluoride (PVDF) membrane, and SliP4 was detected by anti-Flag antibodies. Black-white arrows designate photosystem II (PSII) and subunits assigned according to their characteristic positions (Linhartová *et al.*, 2014); black-white arrows indicate four distinct SliP4.f bands. The designation of complexes: PSI(3) and PSI(1), trimeric and monomeric Photosystem I; PSII(1), monomeric Photosystem II. The control gel with proteins from ΔsliP4 cells is shown as Supporting Information Fig. S4.

Orange and blotted. Complexes present in these two fractions were identified by immunodetection. In fraction 7, the SliP4.f co-migrated with a green supercomplex that we identified as PSI(3)-IsiA by a specific antibody against IsiA. Only a relatively weak signal of SliP4.f was co-localized with PSI(3). By contrast, fraction 9 contained NDH-1L and an additional, smaller NDH complex migrating in the gel to the same position as PSI(1) and PSII(1). The upper SliP4.f band appeared to co-migrate with NDH-1L subunits, the binding partner of the lower-mass SliP4.f signal is however difficult to judge, because it co-migrated with a mixture of complexes mentioned previously (Fig. 4b).

Collectively, results of 2D BN/SDS-PAGE and sucrose gradient with subsequent 2D CN/SDS-PAGE indicate that the dimeric SliP4.f binds to PSI complexes, including PSI(3)-IsiA supercomplexes and possibly also to NDH-1L complex.

SliP4.f is co-purified with PSI, PSII, and NDH-1L

We performed affinity chromatography to verify that SliP4 directly interacts with photosynthetic complexes. To this end, crude extracts from the strain expressing SliP4.f and the *Synechocystis* 6803 WT were loaded on a column specifically binding Flag-tagged proteins. After different washing steps, SliP4.f and associated proteins were eluted and analyzed on native CN gels (Fig. 5). The elution fractions from the SliP4.f-expressing strain displayed bands of green color able to emit fluorescence, whereas the control elutions from WT cells were colorless (Fig. S6). The native CN gels were then separated in a second dimension and stained with Coomassie blue. In the control gel with proteins from WT cells, only some contaminations in the high molecular mass region were detected (Fig. S6), whereas in the SliP4.f elution many clear spots became visible (Fig. 5). The majority of them could be assigned to PSI(1) and PSI(3), to PSII(1) and PSII(2), and to NDH1, particularly the NDH-1L complex, because they were found at positions assigned to these complexes in previous studies (Battchikova *et al.*, 2005). Protein spots that could not be assigned were identified via MS analysis (Table S3). Consistent with our previous results, we found IsiA and NdhD1. These results suggested that SliP4 interacts directly or indirectly with PSI, NDH1, and PSII because proteins from these photosynthetic complexes were completely missing in the WT control experiment (Fig. S6).

As the SliP4 interactome appeared rather complex and it was difficult to judge what might be the primary SliP4-binding partner, we transferred the pVZ322 plasmid expressing SliP4.f into mutants missing either PSI or PSII. Crude extracts from these strains were then used in another affinity purification of Flag-tagged SliP4 and associated proteins. The SliP4.f pulldown, prepared from the cells in PSI-less background, showed a high abundance of PSII(1) and PSII(2) complexes and a relatively high level of NDH1 subunits NdhF1 (*slr0844*) and NdhD1 (*slr0331*). By contrast, the first-dimension gel from the 'PSII-less' pulldown displayed a strong yellow band *c.* 150 kDa that later on was found to be composed of NDH1 subunits NdhF1 and NdhD1 together with two small proteins that were not identified by MS. Given the known structure of NDH1 complexes (Schuller *et al.*, 2019), these proteins are very likely NdhP and NdhQ subunits (Fig. 5c). NdhF1, NdhD1, NdhQ, and NdhP form together the membrane domain of NDH-1L complex that is named here as NDH1 membrane-derived (NDH1_{MD}) subcomplex. Apart from high amounts of NDH1_{MD}, the preparation from PSII-less background also contained a relatively high amount of fully assembled NDH-1L (Fig. 5c). It should be noted that the interaction between SliP4.f and PSI or SliP4.f and NDH1 was at least partially preserved even during CN-PAGE (Fig. 5a,c), while the SliP4.f seems to fully separate from the PSII complexes (Fig. 5b). Altogether, these data fit the pattern of SliP4 complexes observed before in membranes separated by 2D BN/

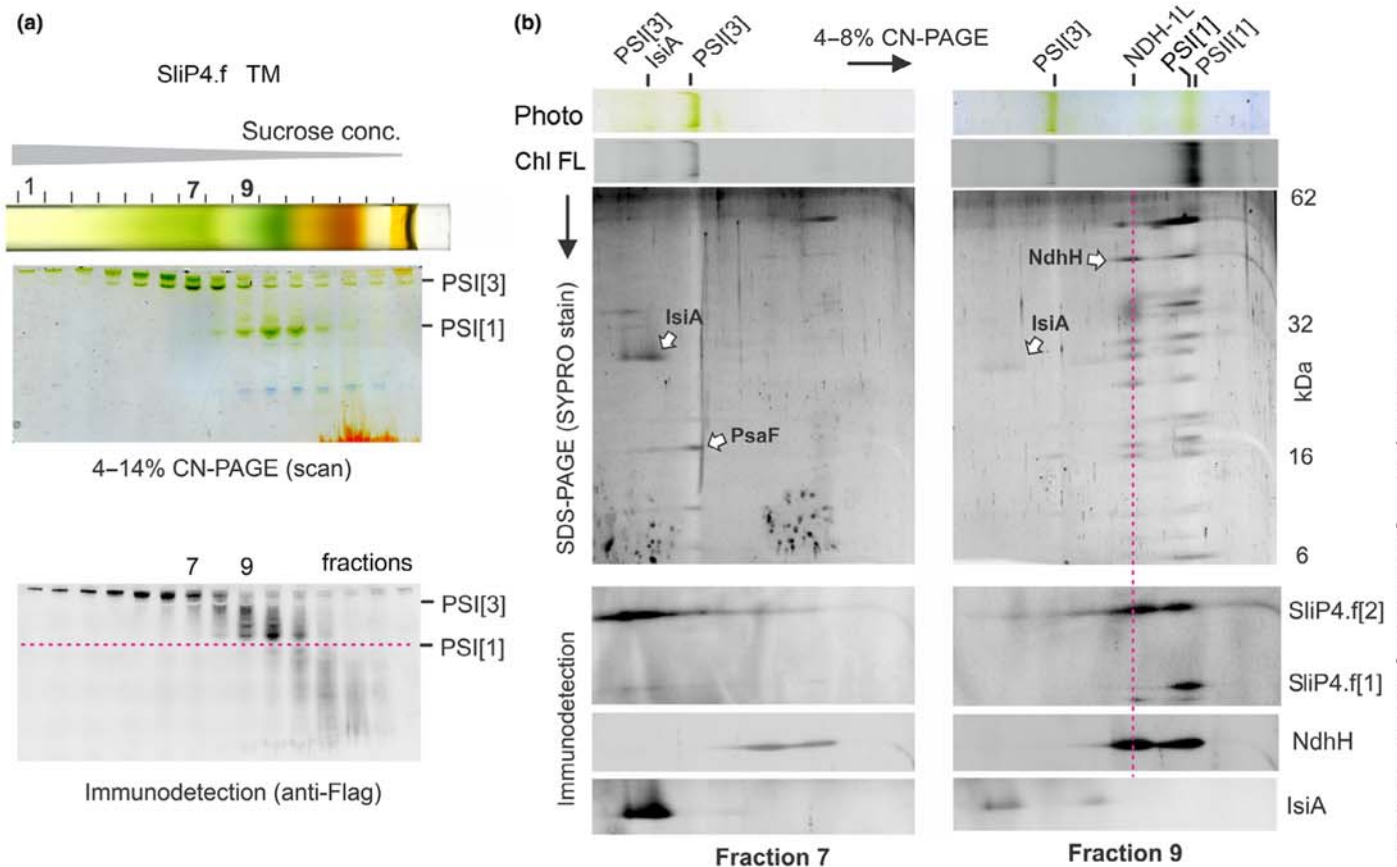


Fig. 4 Fractionation of membrane complexes from *Synechocystis* sp. PCC 6803 on sucrose gradient followed by localization of SliP4.f by CN-PAGE and by Two-dimensional-clear-native/sodiumdodecylsulfate polyacrylamide gel electrophoresis /2D-CN-SDS-PAGE. (a) SliP4.f-expressing cells were grown for 48 h at 250 $\mu\text{mol photons m}^{-2} \text{s}^{-1}$, harvested, broken, and the solubilized membrane proteins separated on sucrose gradients. Collected fractions from sucrose gradient were subsequently analyzed by native 4–14% CN-PAGE; 60 μl of each fraction was loaded onto the gel. After western blotting, SliP4.f was detected by anti-Flag antibody. (b) Fractions 7 and 9 were further separated in the first dimension by CN-PAGE. The native gel was photographed (Photo) and scanned by LAS 4000 (FujiFilm, Tokyo, Japan) for chlorophyll fluorescence (Chl FL). After the second dimension SDS-PAGE, the gel was blotted, and SliP4.f detected by anti-Flag antibody. Please note that a different concentration of acrylamide (4–8%) was used for this experiment to better separate the high-mass complexes. See also Supporting information Fig. S5 for the identical analysis with the control ΔsliP4 strain.

SDS-PAGE (Fig. 3): bands #1 and #2 can be assigned to PSI-IsiA-SliP4 and PSI(3)-SliP4 complexes, while band #3 is most probably PSI(1)-SliP4 and the smallest complex (#4) should be the NDH1_{MD}-SliP4, respectively. Indeed, the highest mass spot observed on BN-PAGE might represent a mixture of several different supercomplexes (see Discussion section).

Recently, several high-resolution NDH-1L structures have been obtained with cryo-electron-microscopy for cyanobacteria (e.g. Laughlin *et al.*, 2019; Schuller *et al.*, 2019; Zhang *et al.*, 2020), which permitted to start modeling the interaction between NDH1_{MD} and SliP4 using ALPHAFOLD multimer (Evans *et al.*, 2021). The model predicted with a high confidence (see Fig. S7A) that SliP4 interacts with the long amphipathic helix of NdhF1 (Fig. 6a,b). According to the model, the binding is stabilized by hydrogen bonds between the NdhF1 Lys613 and Asn24 and Ser32 of SliP4 (Fig. S7B). Because our data strongly suggest that the SliP4 can dimerize, we also modeled dimeric structure of SliP4. The ALPHAFOLD prediction shows that, apart from the hydrophobic interaction of transmembrane helices, the dimeric

structure can be strengthened by the hydrogen bond between Ser21 from each SliP4 chain (Fig. 6c,d).

SliP4 plays an important role in the association of photosynthetic (super)complexes under high-light conditions

The above-described experiments showed that SliP4 is located in thylakoids, in which it is linked/associated with NDH1, PSII, and PSI. Spectroscopic kinetics measurements tracking the PSI redox state were performed to analyze the functional role of SliP4 association with the different photosynthetic complexes. In the first series of experiments, the capacity for cyclic electron transport (CET) was compared in WT and mutant ΔsliP4 after exposure to high light for 24 or 48 h (Fig. 7). CET was measured by reading the oxidation state of PSI after specific excitation with far-red light. Under standard light conditions, the extent of CET was similar in WT and ΔsliP4 . However, upon 24 h high light, the mutant ΔsliP4 displayed weaker CET compared with WT



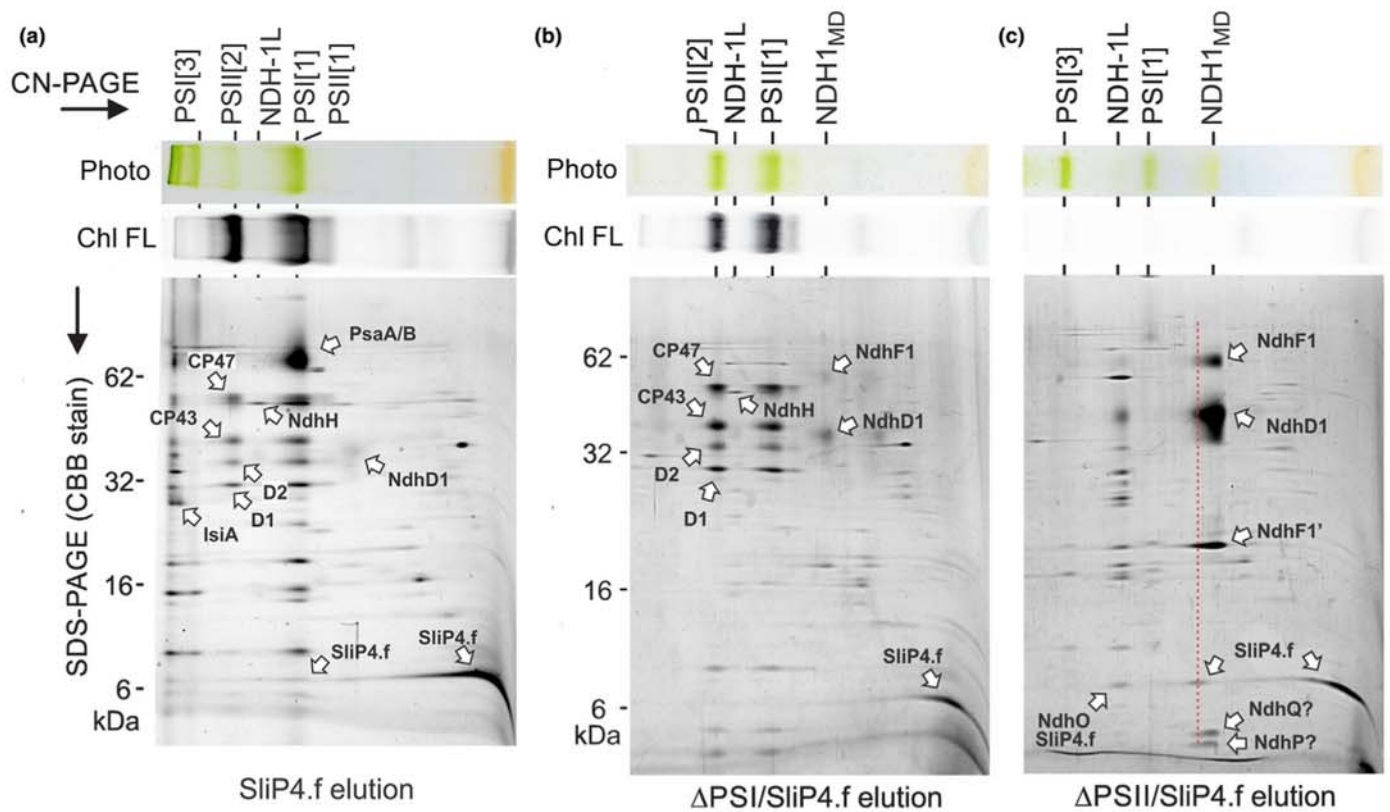


Fig. 5 Two-dimensional-clear-native/sodiumdodecylsulfate polyacrylamide gel electrophoresis (2D-CN/SDS-PAGE) of proteins co-eluted with SliP4.f in different *Synechocystis* sp. PCC 6803 strains. Analysis of the SliP4.f pulldowns obtained from the strain expressing the *sliP4.f* gene in WT background (a), the PSI-less background (b), and PSII-less background (c). SliP4.f cells were pregrown under standard light. To induce the expression of SliP4.f, the irradiance was increased to $150 \mu\text{mol photons m}^{-2} \text{s}^{-1}$ during the last hour of cultivation. To cultivate cells producing SliP4.f but lacking PSI or PSII, strains were grown in BG11 medium supplemented with 5 mM glucose in 10 l flasks at 28°C and $5 \mu\text{mol photons m}^{-2} \text{s}^{-1}$. After purification, the eluted proteins were separated in the first dimension by CN-PAGE. The native gel was photographed (Photo) and scanned by LAS 4000 (FujiFilm) for chlorophyll fluorescence (Chl FL). After the second dimension SDS-PAGE, the gel was stained with Coomassie blue. PSI(1) and PSI(3) mark the monomeric and trimeric forms of PSI, respectively. PSII(1) and PSII(2) mark the monomeric and dimeric forms of PSII, respectively. NDH-1L indicates photosynthetic complex I. Subunits of PSI (PsaA/B) and PSII (D1, D2, CP43, and CP47) are marked based on their typical pattern. NDH_{1MD} indicates the membrane assembly module of photosynthetic complex I. In all three pulldowns NdhD1, NdhF1 and its fragment (NdhF1'), NdhO, and SliP4.f were identified by MS (Supporting Information Table S3). Small NdhP and NdhQ subunits are difficult to identify by MS, but protein bands most likely representing these two subunits are also marked. Red-dashed line highlights the SliP4.f-NDH_{1MD} complex. See Fig. S6 for the control experiment with WT cells.

cells. The WT cells enhanced their capacity for CET after 48 h high-light treatment, whereas this enhancement was not observed in mutant cells (Fig. 7). CET in *Synechocystis* 6803 mainly depends on the so-called NDH-1L route (e.g. Zhang *et al.*, 2020; Hualing, 2022), in which PSI and NDH-1L closely cooperate, which is obviously less possible in high-light-treated mutant cells that is consistent with the above-proven association of SliP4 with PSI and NDH-1L.

Then, we compared the relative activities of the PSI and PSII in different strains at different light intensities. An almost similar increase in the PSI-associated electron transfer rate (ETR) and the PSII-associated ETR with increasing light was observed in WT cells, whereas in the mutant $\Delta sliP4$, the PSI-related ETR relative to PSII was less light responsive (Fig. S8). This difference was not observed in experiments with the complementation strain $\Delta sliP4::SliP4.f$. In this case, the light dependence of ETR from PSI and PSII behaves almost like WT. These measurements indicate that SliP4 also plays a role in coordinating PSI and PSII for linear and cyclic electron flow.

Finally, the capacity for state transition was analyzed in the *Synechocystis* 6803 WT and mutant $\Delta sliP4$. The WT cells showed the expected changes in relative 77 K fluorescence peaks of PSI and PSII depending on the previous light treatment, that is, the light of 600 nm showed preferential emission from the PSII, while this shifted toward PSI after far-red light incubation. In contrast to WT, high-light-treated cells of the mutant $\Delta sliP4$ completely lost the capability to respond to different light qualities with state transitions (Fig. 8). Depending on the model, state transitions are supposed to rely on closer or relaxed association of PSII with PSI and/or phycobilisomes in cyanobacteria (Calzadilla & Kirilovsky, 2020). The absence of SliP4 seems to prevent such a close association.

Moreover, the strain SliP4.f, in which the native *sliP4* gene was knocked out and replaced by the ectopic expression of Flag-tagged SliP4 on the pVZ322 plasmid under the control of the native promoter, displayed slightly higher expression of *sliP4* (data not shown) likely due to a higher gene copy number. Interestingly, this strain also displayed better growth under higher



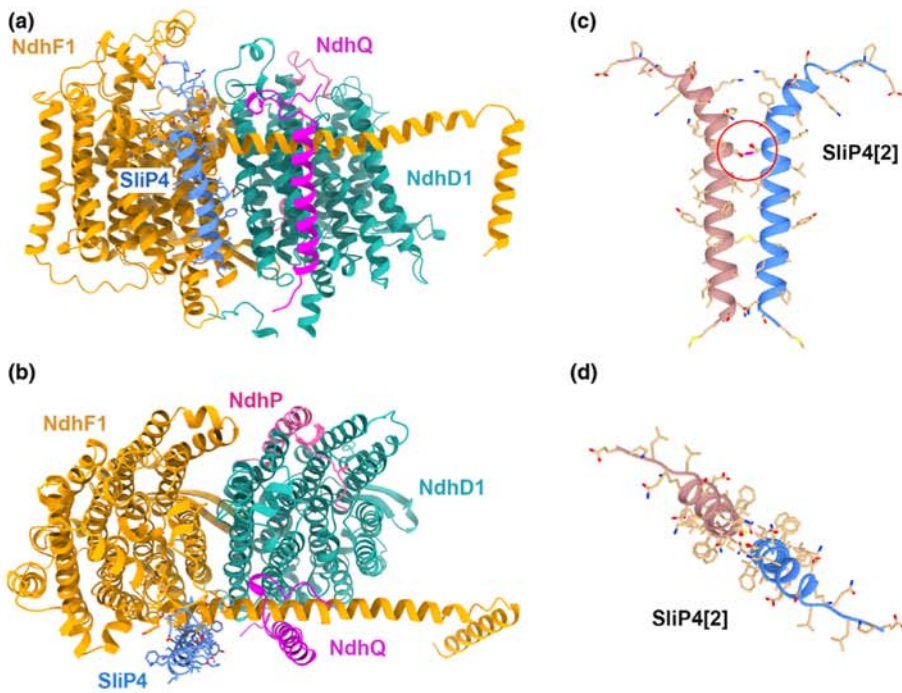


Fig. 6 Structural model of the association of SliP4 with the NDH1 complex and the dimeric SliP4. The model was predicted by AlphaFold multimer (Evans *et al.*, 2021) using *Synechocystis* sp. PCC 6803 SliP4 and NdhF1, NdhD1, NdhQ, and NdhP protein sequences as input. Side view along the membrane plane (a) and a view from the stromal side (b). See Supporting Information Fig. S7 for a more detailed analysis of the predicted structure. (c, d) A prediction of dimeric SliP4 using AlphaFold multimer; hydrogen bond between two Ser21 residues is circled.

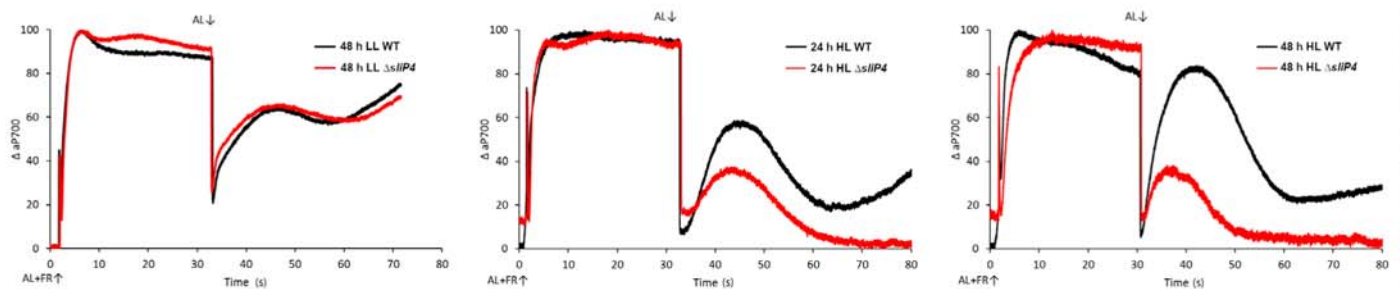


Fig. 7 SliP4 is necessary for enhancing cyclic electron flow around PSI in *Synechocystis* sp. PCC 6803. Cells of the wild-type (WT) and mutant $\Delta sliP4$ were pregrown under low-light conditions (LL) of $50 \mu\text{mol photons m}^{-2} \text{s}^{-1}$ and were then transferred to high-light conditions (HL) of $250 \mu\text{mol photons m}^{-2} \text{s}^{-1}$ for 24 and 48 h, respectively. Slow kinetics of P700 redox changes were measured after the onset of saturating far-red and red actinic light (AL + FR \uparrow) and subsequent switch-off of red actinic light (AL \downarrow) in cells exposed to LL (left panel) and for 24 h (middle panel) or 48 h (right panel) to HL.

light intensities of 300 and $400 \mu\text{mol photons m}^{-2} \text{s}^{-1}$ in comparison with the WT (Fig. S9). Collectively, the observed physiological changes, that is, lowered capacity for cyclic electron flow around PSI, lowered responsiveness of PSI then PSII to different light intensities, and the absence of state transitions in mutant $\Delta sliP4$, support the hypothesis that the association of SliP4 with photosynthetic complexes is involved in their proper organization into cooperative units (supercomplexes), which seems to be particularly important under high-light conditions for *Synechocystis* 6803.

Discussion

Small proteins have been overlooked for a long time. Recently, many of them were discovered, and an increasing body of evidence indicates that they can play important roles, particularly in the proper organization of large protein complexes (reviewed by Hobbs *et al.*, 2011; Storz *et al.*, 2014). A particularly high

number of small proteins has been assigned to the assembly, repair, and function of different photosynthetic complexes in cyanobacteria and chloroplasts of algae and plants (reviewed in Baumgartner *et al.*, 2016; Brandenburg & Klähn, 2020). In the present study, we provide evidence that the newly discovered SliP4 can be regarded as a further example that small proteins are important scaffolds for properly organizing photosynthetic complexes. The expression of *sliP4* is massively upregulated under high-light conditions, and the corresponding mutant unable to accumulate this small protein is more sensitive to high-light shifts than WT cells. This is mainly due to the inability of mutant $\Delta sliP4$ to induce increased CET and to balance energy distribution between PSI and PSII. Our observations support these phenotypes, indicating that SliP4 is specifically interacting with NDH1 and also PSII, thereby coupling these complexes more closely with PSI.

It is well established that the photosynthetic machinery can respond to fluctuating light regimes and the cell's metabolic state

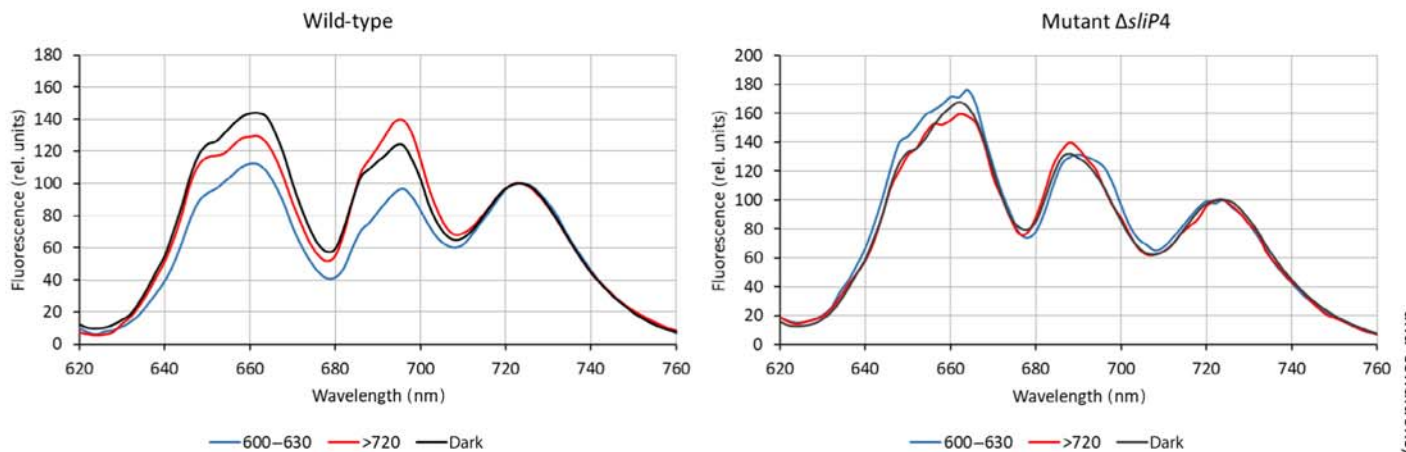


Fig. 8 SliP4 is necessary for state transitions in *Synechocystis* sp. PCC 6803. Cells of the wild-type (WT) and mutant Δ sliP4 were pre-grown under low-light conditions of $50 \mu\text{mol photons m}^{-2} \text{s}^{-1}$ and were then transferred to high-light conditions of $250 \mu\text{mol photons m}^{-2} \text{s}^{-1}$ for 48 h, respectively. Low-temperature (77 K) fluorescence emission spectra of high-light-treated cells were recorded at 600 nm excitation after preincubation in darkness (black line), with far-red light > 720 nm (red line) or with orange light 600–630 nm (blue line).

by reorganizing the amount and composition of photosynthetic complexes (e.g. Nikkanen *et al.*, 2021). In the linear electron transport mode, electrons are conveyed from water via PSII and the cytochrome b_6/f complex to PSI that reduces ferredoxin (Fd) via Fd-NAD(P)H-oxidoreductase, thereby producing NADPH that is mainly used for CO_2 fixation in the Calvin–Benson cycle (CBC). In addition, the electron transport produces an H^+ gradient, which provides the energy for photophosphorylation, that is, ATP production via ATP synthase. There are indications for a cyanobacterial mega-complex of phycobilisomes with PSII and PSI (Liu *et al.*, 2013), which could promote linear electron transport. The NADPH/ATP ratio of linear electron transport does not completely fulfill the CBC's demand. Therefore, CET around PSI is necessary to close the ATP gap. In nature, not only does the amount of light and its quality fluctuate, but also the availability of CO_2 is often limited. The latter is especially relevant for aquatic organisms, such as cyanobacteria and algae, due to the limited solubility of CO_2 in water. Hence, when the sink capacity of the CBC is saturated, the photosynthetic complexes will be excessively reduced, resulting in the generation of reactive oxygen species. The photosystems are vulnerable to excessive reduction. While PSII has a rapid repair cycle, recovery of PSI from damage is slow (Komenda *et al.*, 2012). Therefore, photosynthetic organisms invest heavily in protecting PSI by multiple mechanisms that aim at maintaining PSI and its P700 reaction center chlorophyll pair in an oxidized state.

Photosynthetic organisms can decrease over-reduction by activating auxiliary electron transport pathways that evolved to protect the photosynthetic machinery. The CET and state transition are highly induced processes under such stress conditions (reviewed in Hualing, 2022). CET in cyanobacteria and plant chloroplasts involves NDH1-like complexes, which are phylogenetically related (Battchikova *et al.*, 2011). In chloroplasts, the NDH1-like complex forms a supercomplex with PSI, especially under stress conditions stimulating CET (Peng *et al.*, 2009; Kouril *et al.*, 2014; Shikanai & Yamamoto, 2017). Structural

insights revealed that two copies of PSI-LHCI complexes are associated with one NDH1 and two monomeric LHC1 proteins (Shen *et al.*, 2022; Su *et al.*, 2022). It is assumed that the physical proximity of donor and acceptor complexes appears to be one of the most effective ways to influence the prevalence of different possible electron transport pathways (Mullineaux, 2022).

Our results indicate that SliP4 is likely also involved in the close association of NDH1L and PSI promoting CET in high-light-stressed *Synechocystis* 6803 cells (Fig. 7). There is only limited evidence that PSI-NDH1 supercomplexes might exist in cyanobacteria. Gao *et al.* (2016) provided the best evidence that an NDH1L-PSI supercomplex exists with a molecular mass of more than 1000 kDa in *Synechocystis* 6803. The supercomplex formation is supported by the PSI-specific CpcL phycobilisome (Watanabe *et al.*, 2014), because the screen for high-light-sensitive mutants defective in CET induction identified this gene (Gao *et al.*, 2016). They also showed that the formation of this supercomplex was directly linked to the activity of NDH1-dependent CET (Gao *et al.*, 2016). The exact composition of the cyanobacterial supercomplex is not known. However, Gao *et al.* (2016) speculated that an unknown linker protein, possibly such as the here addressed SliP4, might be involved in the association of PSI and NDH1. Unfortunately, we could not detect the NDH1L-PSI complex reported by Gao *et al.* (2016) using our BN or CN-gel systems. Similarly, to the experimental observation of NDH1L-PSI supercomplexes only in *Synechocystis* 6803 (Watanabe *et al.*, 2014; Gao *et al.*, 2016), the predicted action of SliP4 in high-light-induced photosynthetic supercomplex formation seems also to be restricted to *Synechocystis* 6803 and closely related strains. Clear SliP4 homologs could only be identified in genomes of *Synechocystis* spp. and a few other strains (Figs 1, S1). However, it might be possible that other, not yet identified small proteins with no significant sequence similarity but able to form one transmembrane helix and a polar C-terminal tail could be present in many more cyanobacterial strains and potentially fulfill similar function, which needs to be addressed in future experiments.



In addition to CET, the proper distribution of light energy between the two photosystems via state transition is also implicated in high-light acclimation virtually in all oxygenic phototrophs. While the state transition mechanism is relatively well studied in plants, how state transition operates in cyanobacteria remains unclear. Several models have been proposed such as the migration of the phycobilisome antenna between PSII and PSI or the building of a close phycobilisome PSII and PSI complex in which spillover occurs (Federman *et al.*, 2000; Liu *et al.*, 2013; Calzadilla & Kirilovsky, 2020). Our 77 K fluorescence experiments revealed that cells of the mutant $\Delta sliP4$ could not perform state transition after exposure to high light. This observation suggests that SliP4 facilitates, either directly, or indirectly, this process in *Synechocystis* 6803 (Fig. 8). Our results seem to favor the idea that SliP4 is involved in the closer contact of PSII and PSI to allow spillover of excess light energy (Fig. 9), because no phycobilisome subunits were found in any attempts to identify SliP4 interacting partners, whereas in the PSI-less mutant high amounts of PSII could be co-purified with SliP4.f (Fig. 5). Moreover, while WT and the complementation strain displayed comparable ETR values, $\Delta sliP4$ seems to have problems coupling PSII to PSI (Fig. S8). However, it has also been shown that the NDH1 complex is somehow involved in cyanobacterial state transition, because this process was also completely absent in the M55 mutant with deleted NdhB protein (Schreiber *et al.*, 1995). Hence, the interaction of SliP4 with NDH1 could also explain the missing state transition in mutant $\Delta sliP4$. Furthermore, we cannot rule out that the effect of *sliP4* mutation might be indirect due to a changed redox state of the plastoquinone pool via changed PSI and/or PSII organization. Hence, further experiments are necessary to reveal the specific role of SliP4 in state transition.

The important role of SliP4 in high-light acclimation is documented by the phenotype of the SliP4-null mutant that cannot enhance CET activity under stress conditions. It is, therefore, possible that SliP4 represents a kind of linker stabilizing the attachment of NDH-1L and PSII to PSI complexes (Fig. 9). In addition to this likely explanation, we cannot rule out that the absence of SliP4 impacts the thylakoid membrane ultrastructure, the stability of different photosynthetic complexes, or the formation of PSI-IsiA complexes. The latter function is likely, because PSI-IsiA-SliP4 complexes were observed in WT cells but are virtually absent in the mutant $\Delta sliP4$ (Figs 4, S5). Hence, the impact of *sliP4* deletion can be quite complex and the observed light sensitivity of the mutant can result from pleiotropic effects.

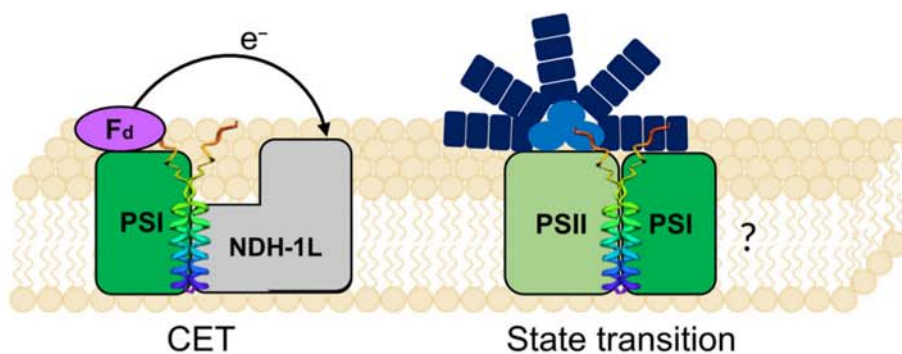


Fig. 9 Likely SliP4 function under high-light conditions. Dimeric SliP4 is capable to attach to photosystem I (PSI), photosystem II (PSII) and also NDH-1L. The polar C-terminal regions of the SliP4 dimer could play an important role in binding of each of these complexes, thereby promoting or stabilizing the formation of PSI-NDH-1L and possibly also PSI-PSII supercomplexes. These large assemblages are needed for an efficient electron transfer during the cyclic electron flow (CET) and energy dissipation during the state transition.



belonging to NdhF1 and NdhD1 but not to other NdhF/D homologs. According to our model of the SliP4-NDH1_{MD} complex (Fig. 6a), SliP4 is located close to NdhQ. This small subunit is specific for the NDH-1L complex and might even be in contact with SliP4, thereby promoting the selectivity of the SliP4 for NDH-1L.

We hypothesize that the highly polar C terminus of SliP4 is important for the interactions with NDH-1L and both photosystems. We failed to obtain a reliable prediction of PSI or PSII associated with SliP4 using AlphaFold, but the SliP4-NDH1_{MD} model supports the key role of C-terminal polar residues. SliP4 could form oligomers, such as a very stable dimer (Figs 3, 6). The binding of two different complexes via C termini of the dimeric SliP4 could work effectively as a protein cross-linker (Fig. 9). SliP4 appears to be essential to healthy electron transfer in the photosynthetic membrane via the coupling of photosystems and NDH1 during high-light exposure.

Acknowledgements

We thank Klaudia Michl, University of Rostock, and Jürgen Bartel, University of Greifswald, for excellent technical assistance. The construction of the initial Δ sliP4 mutant by Dr Vanessa Krauspe (University of Freiburg) and the initial work of Mara Schutz are highly appreciated. We acknowledge the help of Prof. Andreas Richter (Plant Metabolism, University Rostock) during the establishment of BN-gel techniques. This study was funded by the German Research Foundation (DFG) priority program SPP2002 'Small Proteins in Prokaryotes, an Unexplored World' (grant HE 2544/12-2 to WRH, grant HA 2002/22-2 to MH, and grant BE 3869/5-2 to DB) and by the Czech Science Foundation (project 19-29225X) to RS. Open Access funding enabled and organized by Projekt DEAL.

Competing interests

None declared.

Author contributions

LA-L and MH designed the study. LA-L, ML, and RS performed and analyzed pull-down experiments. SM and DB performed and analyzed MS-based proteomics. HS performed and analyzed PAM measurements. LA-L performed the BN gel and physiological analyses. ML performed sucrose gradients and subsequent protein separations. WRH contributed mutant strains and expression data. MH and LA-L drafted the manuscript. All authors read and approved the final manuscript. LA-L and ML contributed equally to this work.

ORCID

Luna Alvarenga-Lucius  <https://orcid.org/0000-0001-7790-6458>

Dörte Becher  <https://orcid.org/0000-0002-9630-5735>

Martin Hagemann  <https://orcid.org/0000-0002-2059-2061>

Wolfgang R. Hess  <https://orcid.org/0000-0002-5340-3423>
 Markéta Linhartová  <https://orcid.org/0000-0002-5148-811X>
 Sandra Maaß  <https://orcid.org/0000-0002-6573-1088>
 Hendrik Schubert  <https://orcid.org/0000-0001-6309-2609>
 Roman Sobotka  <https://orcid.org/0000-0001-5909-3879>

Data availability

The original contributions presented in the study are included in the article and the associated [Supporting Information](#). The proteome datasets have been deposited in the ProteomeXchange Consortium via the PRIDE partner repository (Vizcaíno *et al.*, 2016) with the dataset identifier PXD036788.

References

- Alvarenga LV, Hess WR, Hagemann M. 2020. AcnSP – a novel small protein regulator of aconitase activity in the cyanobacterium *Synechocystis* sp. PCC 6803. *Frontiers in Microbiology* 11: 1445.
- Battchikova N, Eisenhut M, Aro EM. 2011. Cyanobacterial NDH-1 complexes: novel insights and remaining puzzles. *Biochimica et Biophysica Acta* 1807: 935–944.
- Battchikova N, Zhang P, Rudd S, Ogawa T, Aro EM. 2005. Identification of NdhL and Ssl1690 (NdhO) in NDH-1L and NDH-1M complexes of *Synechocystis* sp. PCC 6803. *Journal of Biological Chemistry* 280: 2587–2595.
- Baumgartner D, Kopf M, Klähn S, Steglich C, Hess WR. 2016. Small proteins in cyanobacteria provide a paradigm for the functional analysis of the bacterial micro-proteome. *BMC Microbiology* 16: 285.
- Bolay P, Rozbeh R, Muro-Pastor MI, Timm S, Hagemann M, Florencio FJ, Forchhammer K, Klähn S. 2021. The novel P_{II}-interacting protein PirA controls flux into the cyanobacterial ornithine-ammonia cycle. *mBio* 12: e00229-21.
- Bonn F, Bartel J, Büttner K, Hecker M, Otto A, Becher D. 2014. Picking vanished proteins from the void: how to collect and ship/share extremely dilute proteins in a reproducible and highly efficient manner. *Analytical Chemistry* 86: 7421–7427.
- Brandenburg F, Klähn S. 2020. Small but smart: on the diverse role of small proteins in the regulation of cyanobacterial metabolism. *Life* 10: 322.
- Calzadilla PI, Kirilovsky D. 2020. Revisiting cyanobacterial state transitions. *Photochemical & Photobiological Sciences* 19: 585–603.
- Cox J, Mann M. 2008. MAXQUANT enables high peptide identification rates, individualized p.p.b.-range mass accuracies and proteome-wide protein quantification. *Nature Biotechnology* 26: 1367–1372.
- Dobáková M, Sobotka R, Tichy M, Komenda J. 2009. Psb28 protein is involved in the biogenesis of the photosystem II inner antenna CP47 (PsbB) in the cyanobacterium *Synechocystis* sp. PCC 6803. *Plant Physiology* 149: 1076–1086.
- Evans R, O'Neill M, Pritzel A, Antropova N, Senior A, Green T, Židek A, Bates R, Blackwell S, Yim J *et al.* 2021. Protein complex prediction with AlphaFold-Multimer. *bioRxiv*. doi: 10.1101/2021.10.04.463034.
- Federman S, Malkin S, Scherz A. 2000. Excitation energy transfer in aggregates of Photosystem I and Photosystem II of the cyanobacterium *Synechocystis* sp. PCC 6803: can assembly of the pigment-protein complexes control the extent of spillover? *Photosynthesis Research* 64: 199–207.
- Fridovich I. 1989. Superoxide dismutases: an adaptation to a paramagnetic gas. *Journal of Biological Chemistry* 264: 7761–7764.
- Gao F, Zhao J, Chen L, Battchikova N, Ran Z, Aro EM, Ogawa T, Ma W. 2016. The NDH-1L-PSI supercomplex is important for efficient cyclic electron transport in cyanobacteria. *Plant Physiology* 172: 1451–1464.
- Hagemann M. 2011. Molecular biology of cyanobacterial salt acclimation. *FEMS Microbiology Reviews* 35: 87–123.
- Hagemann M, Song S, Brouwer EM. 2021. Inorganic carbon assimilation in cyanobacteria: mechanisms, regulation, and engineering. In: Nielsen J, Lee S, Stephanopoulos G, Hudson P, eds. *Cyanobacteria biotechnology*. Weinheim, Germany: Wiley-VCH GmbH, 1–31.



- Hobbs EC, Fontaine F, Yin X, Storz G. 2011. An expanding universe of small proteins. *Current Opinion in Microbiology* 14: 167–173.
- Hohmann-Marriott MF, Blankenship RE. 2011. Evolution of photosynthesis. *Annual Reviews in Plant Biology* 62: 515–548.
- Hör J, Matera G, Vogel J, Gottesman S, Storz G. 2020. Trans-acting small RNAs and their effects on gene expression in *Escherichia coli* and *Salmonella enterica*. *EcoSal Plus* 9: 1–35.
- Hualing M. 2022. Cyanobacterial NDH-1 complexes. *Frontiers in Microbiology* 13: 933160.
- Jackson PJ, Hitchcock A, Brindley AA, Mark J, Dickman MJ, Hunter CN. 2023. Absolute quantification of cellular levels of photosynthesis-related proteins in *Synechocystis* sp. PCC 6803. *Photosynthesis Research* 155: 219–245.
- Janknegt PJ, Rijstenbil JW, Van de Poll WH, Gechev TS, Buma AG. 2007. A comparison of quantitative and qualitative superoxide dismutase assays for application to low temperature microalgae. *Journal of Photochemistry and Photobiology B: Biology* 87: 218–226.
- Jeong Y, Hong SJ, Cho SH, Yoon S, Lee H, Choi HK, Kim DM, Lee CG, Cho S, Cho BK. 2021. Multi-omic analyses reveal habitat adaptation of marine cyanobacterium *Synechocystis* sp. PCC 7338. *Frontiers in Microbiology* 12: 667450.
- Kameo S, Aso M, Furukawa R, Matsumae R, Yokono M, Fujita T, Tanaka A, Tanaka R, Takabayashi T. 2021. Substitution of deoxycholate with the amphiphilic polymer Amphipol A8-35 improves the stability of large protein complexes during native electrophoresis. *Plant and Cell Physiology* 62: 348–355.
- Kaneko T, Sato S, Kotani H, Tanaka A, Asamizu E, Nakamura Y, Miyajima N, Hirose M, Sugiura M, Sasamoto S *et al.* 1996. Sequence analysis of the genome of the unicellular cyanobacterium *Synechocystis* sp. strain PCC6803. II. Sequence determination of the entire genome and assignment of potential protein-coding regions. *DNA Research* 3: 109–136.
- Klähn S, Höhne A, Simon E, Hagemann M. 2010. The gene *sl3076* encodes a protein mediating the salt-induced expression of *ggpS* for the biosynthesis of the compatible solute glucosylglycerol in *Synechocystis* sp. strain PCC 6803. *Journal of Bacteriology* 192: 4403–4412.
- Komenda J, Knoppová J, Kopečná J, Sobotka R, Halada P, Yu J, Nickelsen J, Boehm M, Nixon PJ. 2012. The Psb27 assembly factor binds to the CP43 complex of photosystem II in the cyanobacterium *Synechocystis* sp. PCC 6803. *Plant Physiology* 158: 476–486.
- Kopf M, Klähn S, Pade N, Weingärtner M, Hagemann M, Voß B, Hess WR. 2014a. Comparative genome analysis of the closely related *Synechocystis* strains PCC 6714 and PCC 6803. *DNA Research* 21: 255–266.
- Kopf M, Klähn S, Scholz I, Matthiessen JKF, Hess WR, Voß B. 2014b. Comparative analysis of the primary transcriptome of *Synechocystis* sp. PCC 6803. *DNA Research* 21: 527–539.
- Koskela MM, Skotnicová P, Kiss É, Sobotka R. 2020. Purification of protein-complexes from the cyanobacterium *Synechocystis* sp. PCC 6803 using FLAG-affinity chromatography. *Bio-Protocol* 10: e3616.
- Kouřil R, Strouhal O, Nosek L, Lenobel R, Chamrád I, Boekema EJ, Šebela M, Ilík P. 2014. Structural characterization of a plant photosystem I and NAD (P) H dehydrogenase supercomplex. *The Plant Journal* 77: 568–576.
- Laughlin TG, Bayne AN, Trempe JF, Savage DF, Davies KM. 2019. Structure of the complex I-like molecule NDH of oxygenic photosynthesis. *Nature* 566: 411–414.
- Laughlin TG, Savage DF, Davies KM. 2020. Recent advances on the structure and function of NDH-1: the complex I of oxygenic photosynthesis. *Biochimica et Biophysica Acta (BBA)-Bioenergetics* 1861: 148254.
- Linhartová M, Bučinská L, Halada P, Ječmen T, Šetlík J, Komenda J, Sobotka R. 2014. Accumulation of the type IV prepillin triggers degradation of SecY and YidC and inhibits synthesis of Photosystem II proteins in the cyanobacterium *Synechocystis* PCC 6803. *Molecular Microbiology* 93: 1207–1223.
- Liu H, Chen J, Huang RYC, Weisz D, Gross ML, Pakrasi HB. 2013. Mass spectrometry-based footprinting reveals structural dynamics of loop E of the chlorophyll-binding protein CP43 during photosystem II assembly in the cyanobacterium *Synechocystis* 6803. *Journal of Biological Chemistry* 288: 14212–14220.
- Mantovani O, Reimann V, Haffner M, Herrmann FP, Selim KA, Forchhammer K, Hess WR, Hagemann M. 2022. The impact of the cyanobacterial carbon-regulator protein SbtB and of the second messengers cAMP and c-di-AMP on CO₂-dependent gene expression. *New Phytologist* 234: 1801–1816.
- Mullineaux CW. 2022. Improving the transport of electrons. In: Ruban A, Foyer CH, Murchie EH, eds. *Photosynthesis in action*. London, UK: Academic Press, 161–174.
- Nikkanen L, Solymosi D, Jokel M, Allahverdiyeva Y. 2021. Regulatory electron transport pathways of photosynthesis in cyanobacteria and microalgae: recent advances and biotechnological prospects. *Physiologia Plantarum* 173: 514–525.
- Orthwein T, Scholl J, Spät P, Lucius S, Koch M, Macek B, Hagemann M, Forchhammer K. 2021. The novel PII-interactor PirC identifies phosphoglycerate mutase as key control point of carbon storage metabolism in cyanobacteria. *Proceedings of the National Academy of Sciences, USA* 118: e2019988118.
- Pakrasi HB, Williams JG, Arntzen CJ. 1988. Targeted mutagenesis of the *psbE* and *psbF* genes blocks photosynthetic electron transport: evidence for a functional role of cytochrome b559 in photosystem II. *EMBO Journal* 7: 325–332.
- Peng L, Fukao Y, Fujiwara M, Takami T, Shikanai T. 2009. Efficient operation of NAD(P)H dehydrogenase requires supercomplex formation with photosystem I via minor LHCl in Arabidopsis. *Plant Cell* 21: 3623–3640.
- Ponce-Toledo RI, Deschamps P, López-García P, Zivanovic Y, Benzerara K, Moreira D. 2017. An early-branching freshwater cyanobacterium at the origin of plastids. *Current Biology* 27: 386–391.
- Prommeenate P, Lennon AM, Markert C, Hippler M, Nixon PJ. 2004. Subunit composition of NDH-1 complexes of *Synechocystis* sp. PCC 6803: identification of two new *ndh* gene products with nuclear-encoded homologues in the chloroplast Ndh complex. *The Journal of Biological Chemistry* 279: 28165–28173.
- Rippka R, Deruelles J, Waterbury JB, Herdman M, Stanier RY. 1979. Generic assignments, strain histories and properties of pure cultures of cyanobacteria. *Microbiology* 111: 1–61.
- Schreiber U, Endo T, Mi H, Asada K. 1995. Quenching analysis of chlorophyll fluorescence by the saturation pulse method: particular aspects relating to the study of eukaryotic algae and cyanobacteria. *Plant and Cell Physiology* 36: 873–882.
- Schuller JM, Birrell JA, Tanaka H, Konuma T, Wulffhorst H, Cox N, Schuller SK, Thiemann J, Lubitz W, Sétif P *et al.* 2019. Structural adaptations of photosynthetic complex I enable ferredoxin-dependent electron transfer. *Science* 363: 257–260.
- Schwarz D, Schubert H, Georg J, Hess WR, Hagemann M. 2013. The gene *sm10013* of *Synechocystis* species strain PCC 6803 encodes for a novel subunit of the NAD(P)H oxidoreductase or complex I that is ubiquitously distributed among cyanobacteria. *Plant Physiology* 163: 1191–1202.
- Shen G, Boussiba S, Vermaas WF. 1993. *Synechocystis* sp. PCC 6803 strains lacking photosystem I and phycobilisome function. *Plant Cell* 5: 1853–1863.
- Shen L, Tang K, Wang W, Wang C, Wu H, Mao Z, An S, Chang S, Kuang T, Shen JR *et al.* 2022. Architecture of the chloroplast PSI–NDH supercomplex in *Hordeum vulgare*. *Nature* 601: 649–654.
- Shikanai T, Yamamoto H. 2017. Contribution of cyclic and pseudo-cyclic electron transport to the formation of proton motive force in chloroplasts. *Molecular Plant* 10: 20–29.
- Sigalat C, de Kouchkovsky Y. 1975. Fractionnement et caractérisation de l'appareil photosynthétique de l'algue bleue unicellulaire *Anacystis nidulans*. I. Obtention de fractions par lyse osmotique et analyse pigmentaire. *Physiologie végétale* 13: 243–258.
- Song K, Baumgartner D, Hagemann M, Muro-Pastor AM, Maass S, Becher D, Hess WR. 2022. Atp^o is an inhibitor of F₀F₁ ATP synthase to arrest ATP hydrolysis during low-energy conditions in cyanobacteria. *Current Biology* 32: 136–148.
- Storz G, Wolf YI, Ramamurthi KS. 2014. Small proteins can no longer be ignored. *Annual Reviews in Biochemistry* 83: 753–777.
- Su X, Cao D, Pan X, Shi L, Liu Z, Dall'Osto L, Bassi R, Zhang X, Li M. 2022. Supramolecular assembly of chloroplast NADH dehydrogenase-like complex with photosystem I from *Arabidopsis thaliana*. *Molecular Plant* 15: 454–467.
- Trautmann D, Voss B, Wilde A, Al-Babili S, Hess WR. 2012. Microevolution in cyanobacteria: re-sequencing a motile strain of *Synechocystis* sp. PCC 6803. *DNA Research* 19: 435–448.



- Vizcaíno JA, Csordas A, Del-Toro N, Dianas JA, Griss J, Lavidas I, Mayer G, Perez-Riverol Y, Reisinger F, Ternent T *et al.* 2016. 2016 update of the PRIDE database and its related tools. *Nucleic Acids Research* 44: D447–D456.
- Watanabe M, Semchonok DA, Webber-Birungi MT, Ehira S, Kondo K, Narikawa R, Ohmori M, Boekema EJ, Ikeuchi M. 2014. Attachment of phycobilisomes in an antenna–photosystem I supercomplex of cyanobacteria. *Proceedings of the National Academy of Sciences, USA* 111: 2512–2517.
- Wilson A, Boulay C, Wilde A, Kerfeld CA, Kirilovsky D. 2007. Light-induced energy dissipation in iron-starved cyanobacteria: roles of OCP and IsiA proteins. *Plant Cell* 19: 656–672.
- Wulfhorst H, Franken LE, Wessinghage T, Boekema EJ, Nowaczyk MM. 2014. The 5 kDa protein NdhP is essential for stable NDH-1L assembly in *Thermosynechococcus elongatus*. *PLoS ONE* 9: e103584.
- Zhang C, Shuai J, Ran Z, Zhao J, Wu Z, Liao R, Wu J, Ma W, Lei M. 2020. Structural insights into NDH-1 mediated cyclic electron transfer. *Nature Communications* 11: 888.

Supporting Information

Additional Supporting Information may be found online in the Supporting Information section at the end of the article.

Fig. S1 Multiple sequence alignment of 19 putative SliP4 homologs.

Fig. S2 Genotyping of the different mutants.

Fig. S3 Testing a functional link between SliP4 and SodB.

Fig. S4 2D-analysis of membrane proteins of the *Synechocystis* sp. PCC 6803 Δ sliP4 strain.

Fig. S5 Fractionation of membrane complexes from the *Synechocystis* sp. PCC 6803 Δ sliP4 strain on sucrose gradient.

Fig. S6 2D CN/SDS-PAGE of the control Flag affinity pulldown using the *Synechocystis* sp. PCC 6803 wild-type (WT) strain.

Fig. S7 Structural model of the association of SliP4 with the NDH1 complex and the dimeric SliP4.

Fig. S8 SliP4 is necessary for proper association of PSI and PSII in linear electron flow in *Synechocystis* sp. PCC 6803.

Fig. S9 Growth curve of the *Synechocystis* sp. PCC 6803 wild-type (WT) and the SliP4.f-expressing strains under higher light intensities.

Table S1 Strains used in the present study.

Table S2 Primers used in the present study.

Table S3 Bands used for MS analysis from 2D CN/SDS-gels of *Synechocystis* sp. PCC 6803 strains with respective identifications.

Please note: Wiley is not responsible for the content or functionality of any Supporting Information supplied by the authors. Any queries (other than missing material) should be directed to the *New Phytologist* Central Office.

